16116 *Biochemistry* **1998,** *37,* 16116−16129

Equilibrium Unfolding (Folding) Pathway of a Model H-type Pseudoknotted RNA: The Role of Magnesium Ions in Stability†

Paul L. Nixon and David P. Giedroc*

Department of Biochemistry and Biophysics, Center for Macromolecular Design, Texas A&M University,
College Station, Texas 77843-2128

Received July 17, 1998; Revised Manuscript Received September 4, 1998

ABSTRACT: In T2 and related T-even bacteriophages, the upstream autoregulatory mRNA leader sequence of gene *32* folds into a simple tertiary structural motif, a hairpin (H)-type pseudoknot. This pseudoknot is derived from 32 contiguous nucleotides which form two coaxially stacked helical stems that adopt a pseudocontinuous A-form helical structure. These stems are connected by two nonequivalent single-stranded loops. The equilibrium unfolding pathway of a 36-nucleotide RNA fragment corresponding to the wild-type and sequence variants of the T2 gene *32* mRNA pseudoknot has been probed as a function of [Mg^{2+}] by analysis of dual optical wavelength, equilibrium thermal melting profiles. A van't Hoff model based on multiple sequential, two-state unfolding transitions has been applied to the resultant data. Compensatory base pair substitutions incorporated into the helical stems have been used to assign optical melting transitions to molecular unfolding events. The optical melting profile of the wild-type RNA is minimally described by three sequential unfolding transitions. The helix−helix junction region melts first in a low-enthalpy transition, followed by the unfolding of the remainder of helical stem 2, and then, all of stem 1. The total enthalpy of unfolding (folding) at [Mg^{2+}] ≥ 1 mM is accounted for by the secondary structure alone, suggesting that, if any non-Watson−Crick or tertiary structure exists in this conformation, it makes little or no enthalpic contribution to the stability of the molecule. Consistent with this, the [Mg^{2+}] dependence of individual unfolding transitions within the pseudoknot is well-described by differential extents of delocalized binding of Mg^{2+} to folded and unfolded regions of the molecule. At a fixed [Mg^{2+}], the helix junction region and stem 2 sequester more Mg^{2+} ions than the stem 1 hairpin; a larger fraction of these ions are then released upon unfolding. Two base or base pair substitution mutant RNAs which destabilize the helical junction and/or the base of stem 2 appear to sequester fewer ions, with a correspondingly smaller number of these ions released upon unfolding.

Recent crystallographic and solution structures of regulatory and catalytic RNAs have greatly increased our understanding of RNA tertiary structure (*1*−*5*). RNA pseudoknots, formed by Watson−Crick base pairing between hairpin or bulge loops and a single-stranded region or the same RNA molecule, are emerging as a common structural motif in RNAs which function in catalysis, molecular recognition, and translational regulation (*6*−*10*). While continued refinement of the nearest-neighbor model of RNA folding allows for increasingly accurate secondary structure predictions (*11*−*13*; for a review, see ref *14*), comparatively little is known about the energetics of formation of non-Watson−Crick base pairing and RNA tertiary structures, as well as the importance of loop-closing entropies, in complex RNA molecules (*15*). RNA tertiary structures or other non-nearest-neighbor or nonlocal interactions can, in effect, stabilize otherwise unstable secondary structural units. For example, the tertiary structural core of a conserved 23S ribosomal RNA which corresponds to the binding site of L11 is an example of just this type of behavior, in which a helical stem, when excised from the rest of the molecule, adopts a non-native structure (*16*). In addition, the presence of a defined RNA tertiary structure can dramatically affect the conformational equilibrium of an RNA molecule, an example of which is the complex α-mRNA pseudoknot (*17*, *18*). Since pseudoknots represent a simple and widely recognized building block employed by RNA to create large and complex globular structures (e.g., the group I intron) (*19*), an understanding of RNA folding begins with an understanding of the factors which contribute to the thermodynamic stability of RNA pseudoknots.

The objective of this and previous work (*20*) is to use the T-even gene *32* mRNA autoregulatory pseudoknot (*7*, *21*) as a model system (*20*, *22*, *23*) to define structure−stability determinants in H-type pseudoknots, and in particular, the extent to which tertiary structure or other non-nearest-neighbor or non-Watson−Crick interactions stabilize this simple folded conformation. A low-resolution structural model of the T2-derived gene *32* mRNA pseudoknot (*23*) has recently been refined to higher resolution (*24*). Both T4- and T2-derived pseudoknots contain two coaxially stacked helical stems (1 and 2), connected by two nonequivalent loops, a

---

† This work supported by NIH Grant AI40187 to D.P.G. and D. W. Hoffman.

* To whom all correspondence should be addressed. Tel: 409-845-4231. Fax: 409-862-4718. E-mail: giedroc@tamu.edu.

[1] P. L. Nixon and D. P. Giedroc (submitted for publication).

10.1021/bi981726z CCC: $15.00

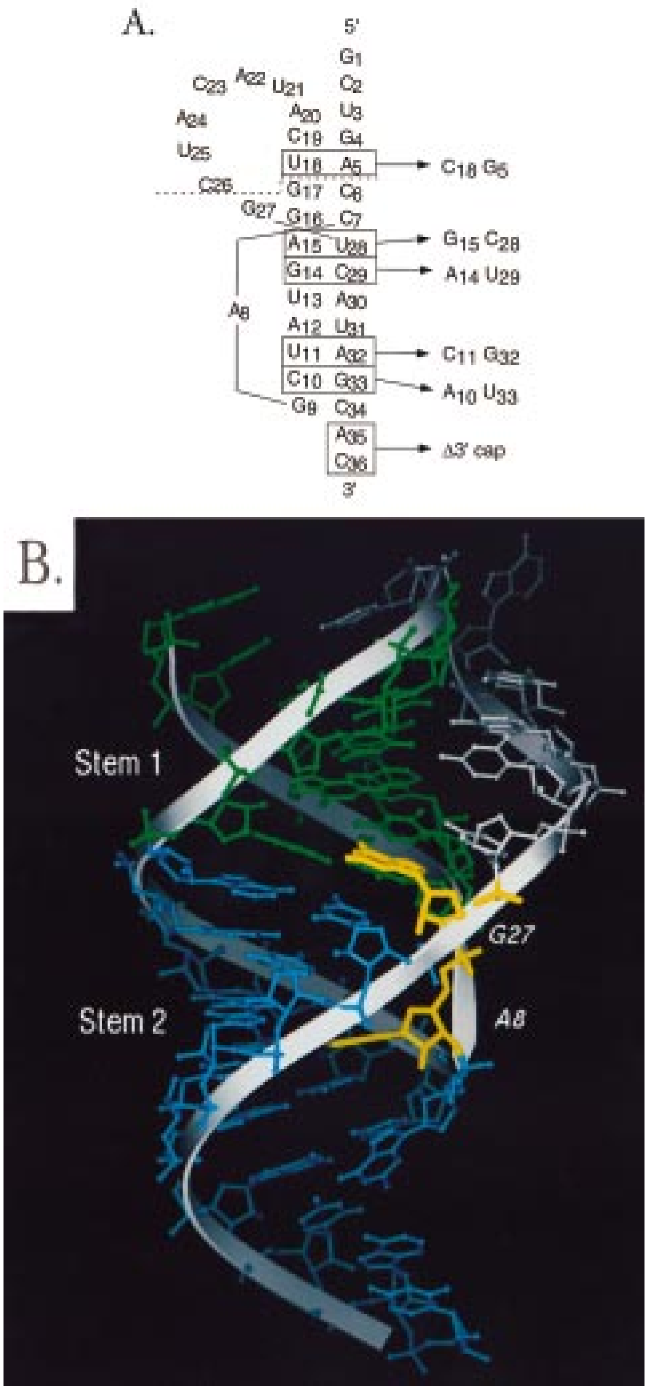

FIGURE 1: (A) Folded pseudoknot representation of the wild-type bacteriophage T2 RNA with the single nucleotide and base pair substitution and deletion mutants characterized in this study. (B) Structural model of the T2 pseudoknot calculated from the solution NMR distance and dihedral angle constraints with the conformation of only the middle of the two stems (stem 1, G17-C6 through A20-U3; stem 2, C10-G33 through G14-C29) restricted to A-helical structure (*23, 24*). These calculations define the overall fold of the molecule and establish that the helix−helix junction involves coaxial stacking of the stems with a helix−helix bend angle of 15° ± 15° (*24*). They do not uniquely place A8 or G27 in the structure of the molecule.

single adenosine-containing loop 1 which crosses the major groove of stem 2, and a larger loop 2 which traverses the minor groove of stem 1 (Figure 1B). One recently reported solution structure of a plant viral RNA pseudoknot revealed some well-defined interactions between the helical stems and the single-stranded loops, particularly at or near the helix−helix junction (*3*).

Our basic strategy is to use mutant RNAs containing compensatory base pair substitutions in the helical stems to define the unfolding pathway, followed by analyzing the effect that single-stranded nucleotide substitution and deletions have on the unfolding pathway in order to probe and quantify the effects of potential loop−stem interactions. Our previous studies (*20*) showed that the optical melting profile of the T4 gene *32* pseudoknot was well-described by the sequential unfolding of the two helical stems, with the weaker of the two stems unfolding first, and the total enthalpy of unfolding essentially that predicted from secondary structure alone. This is direct evidence that, enthalpically, any thermodynamic coupling outside of coaxial stacking of the two helical stems is weak, and certainly not on the order of that observed in folded RNAs with well-defined tertiary structure, for example, transfer RNA (*25*) and ribosomal RNAs (*16*). Another study on a read-through mRNA pseudoknot reached the same conclusion (*18*). However, the nature of the nucleotide in loop 1 and the immediately adjacent 3′ single-stranded helical cap (Figure 1B) do not play passive roles in stability since substitution or deletion of these nucleotides was found to globally destabilize the molecule by about ∼1 kcal mol^{-1} at 37 °C. This is significant since the global stability of the pseudoknotted conformation in this case was only 1−1.5 kcal mol^{-1} more stabile that the partially folded stem 2 hairpin structure (*20*).

In this and other work[1] we report analogous studies of the bacteriophage T2 mRNA pseudoknot. We make the surprising finding that the unfolding pathway of the T2 pseudoknot contrasts sharply with that of the T4 molecule. Defining this pathway has allowed us to obtain a thermodynamic understanding of the role that magnesium ions play in strongly stabilizing this conformation, as well as to determine the extent to which potential single-stranded RNA−duplex RNA interactions contribute to the local and global stability of this conformation.[1]

MATERIALS AND METHODS

RNA Synthesis and Purification. RNAs with the sequences shown in Figure 1A were prepared by in vitro transcription using T7 RNA polymerase and partially double-stranded templates as described (*22*, *23*). Crude RNAs were purified by denaturing PAGE,[2] visualized by UV shadowing, and electroeluted using an S&S electroeluter. The recovered RNA was loaded onto a C18 cartridge (Alltech), eluted with a 50% methanol wash, taken to dryness, and subjected to exhaustive dialysis against 10 mM MOPS, pH 7.0, and 0.10 M KCl. The first change of dialysis buffer contained 10 mM EDTA, with subsequent (3−4) changes containing no added chelator. RNAs were stored at −70 °C until use. Samples were prepared for thermal denaturation by diluting into final dialysis buffer, adding the appropriate concentration of MgCl_2, heating at 65 °C for 10 min, and then slow cooling to room temperature.

---

[2] Abbreviations: MOPS, 3-[*N*-morpholino]propanesulfonic acid; EDTA, ethylenediaminetetraacetic acid; PAGE, polyacrylamide gel electrophoresis.

Thermal Denaturation Experiments. All RNA melts were collected on a Cary 1 spectrophotometer equipped with a temperature controller operating in double-beam mode. Unless otherwise indicated, all melts were collected in 10 mM MOPS, pH 7.0, and 0.10 M KCl with the indicated concentration of $MgCl_2$ added. Capped cells were used, and percent transmittance was recorded as a function of temperature at both 260 and 280 nm simultaneously. Samples were loaded into room-temperature cuvettes and the cells allowed to equilibrate at 2 °C for 30 min. The temperature controller was ramped at a rate of 0.3 °C/min from 2 to 100 °C. Data points were collected every 0.3−0.4 °C as determined by a temperature probe inserted into a cuvette containing final dialysis buffer.

Analysis of the Thermal Melting Profiles. Cary 1 report files were converted from percent transmittance to absorbance and subjected to piece-wise linear interpolation. The interpolated sets of data were then smoothed over an approximately 4 °C window, and the melting profile was generated by taking the first derivative of absorbance with respect to temperature ($\partial A/\partial T$) and plotted as a function of temperature. Melting profiles were subjected to nonlinear least-squares parameter estimation of $t_{m,i}$, ΔH_i, and A_i, for each *i*th sequential unfolding transition via application of a multi-transition, sequential unfolding model using the t-melt program running on an SGI O_2 unix or a PC−Linux workstation exactly as described previously (*16*, *20*). A four transition, unbiased fit was applied to all melting profiles in which $t_{m,i}$, ΔH_i, and A_i were unconstrained. In instances where this failed due to limitations of the fitting model, the melting profile was fit to four independent transitions with no constraints. In a second sequential fit, the parameters obtained from the independent transition fit were then used to weakly constrain either $t_{m,i}$ or ΔH_i for the transitions that had previously failed to converge to unique values in the sequential fit.

Analysis of the Magnesium Concentration Dependence of the Melting Profiles. We have used the general equation derived by Laing et al. (*26*) from Schellman (*27*) which accounts for the change in t_m of a two-state RNA unfolding transition when Mg^{2+} binds to multiple sites on the folded and unfolded conformations. This model assumes that each phosphate can become a binding site for a Mg^{2+} ion and that one ion interacts electrostatically with two phosphates (excluded site size, $n = 2$) (*28*):

$$Z_f = [0.5 + 0.5(1 + 4K_fL)^{1/2}]^m \tag{1}$$

$$Z_u = [0.5 + 0.5(1 + 4K_uL)^{1/2}]^m \tag{2}$$

where Z_f and Z_u are binding polynomials for the excluded site binding of Mg^{2+} to the folded and unfolded forms of the RNA, respectively; L is the free [Mg^{2+}]; K_f and K_u are the equilibrium affinities of a Mg^{2+} ion for the folded and unfolded RNAs, respectively; and m is the number of phosphates participating in the unfolding transition (*26*). If K_o is defined as the unfolding equilibrium constant of a particular two-state unfolding transition in the absence of Mg^{2+} (at some monovalent salt concentration, temperature, and pH), Schellman (*27*) has shown that the natural log of K_{obs}, the observed unfolding equilibrium constant at some [Mg^{2+}], is simply the following

$$\ln K_{obs} = \ln K_o + \ln Z_u - \ln Z_f \tag{3}$$

The t_m of the unfolding transition is the temperature at which $K_{obs} = 1$. From the van't Hoff relationship,

$$\ln K_o = (\Delta H_o/R)(1/t_o - 1/t_m) \tag{4}$$

where t_o is the melting temperature in the absence of Mg^{2+} and t_m is melting temperature at some [Mg^{2+}], substitution of eq 4 into eq 3 and rearrangement gives:

$$1/t_m = 1/t_o - (R/\Delta H_o) \ln(Z_f/Z_u) \tag{5}$$

The derivative of $\ln Z_i$ with respect to $\ln L$ is simply the binding isotherm which relates extent of [Mg^{2+}] binding, ν_i, to L (*29*):

$$\nu_i = \partial \ln Z_i/\partial \ln L = 2mK_iL/\{(1 + 4K_iL)^{1/2} + (1 + 4K_iL)\} \tag{6}$$

RESULTS

To define the thermodynamics of unfolding for the T2 pseudoknot, the compensatory base pair substitution or deletion mutants shown in Figure 1A were prepared and characterized. For structural reference, a ribbon representation of the three-dimensional solution structure of the wild-type 36-nucleotide T2 pseudoknot is shown in Figure 1B (*23*).[1]

Optical Melting Profiles of the Wild-Type T2 Pseudoknot. Complete optical melting and cooling profiles acquired at 260 and 280 nm (plotted as $\partial A/\partial T$ vs T) for the wild-type 36-nucleotide T2 pseudoknot in the absence of exogenously added Mg^{2+} in 0.10 M K^+ are shown in Figure 2 with the thermodynamic parameters collected in Table 1. Examination of the melting and cooling profiles reveals that they are essentially superimposable, consistent with fully reversible behavior. In addition, the melting profiles are independent of scan rate between 0.2 and 1.0 °C/min, indicative of equilibrium unfolding behavior (data not shown). In this and all cases, the experimental data are presented in the left-hand side of each panel and are superimposed with a solid curve which describes an optimized nonlinear least-squares fit to an unfolding model consisting of four sequential, two-state transitions, with the van't Hoff enthalpies (ΔH), t_m's, and hyperchromicity ratios (A_{260}/A_{280}) compiled in Table 1. In each panel, individual transition fits are shown on the right-hand side of the figure for clarity. The first unfolding transition, under these conditions, is a broad low-enthalpy transition clearly visible in these and all other melts collected under conditions of high monovalent or divalent cation concentration (see below). This is followed by two major transitions, which are somewhat close on the temperature coordinate. The first major transition has a ΔH of 35 kcal mol^{-1}, a t_m of 52 °C, and more 260 nm hyperchromicity than 280 nm (A_{260}/A_{280} ratio $\approx$ 2.0). In contrast, the second major transition is characterized by a ΔH of 43 kcal mol^{-1}, a t_m of 66 °C, and more 280 nm than 260 nm hyperchromicity (A_{260}/A_{280} ratio $\approx$ 0.7). This melting profile is qualitatively similar to preliminary work published previously (*23*).

Optical melting profiles are shown in Figure 2 (lower panels) for the stem 2 hairpin fragment, Δ(1−8) T2 (T2HP), which is incapable of forming the pseudoknot. Although there is a low-enthalpy, low-amplitude transition before the

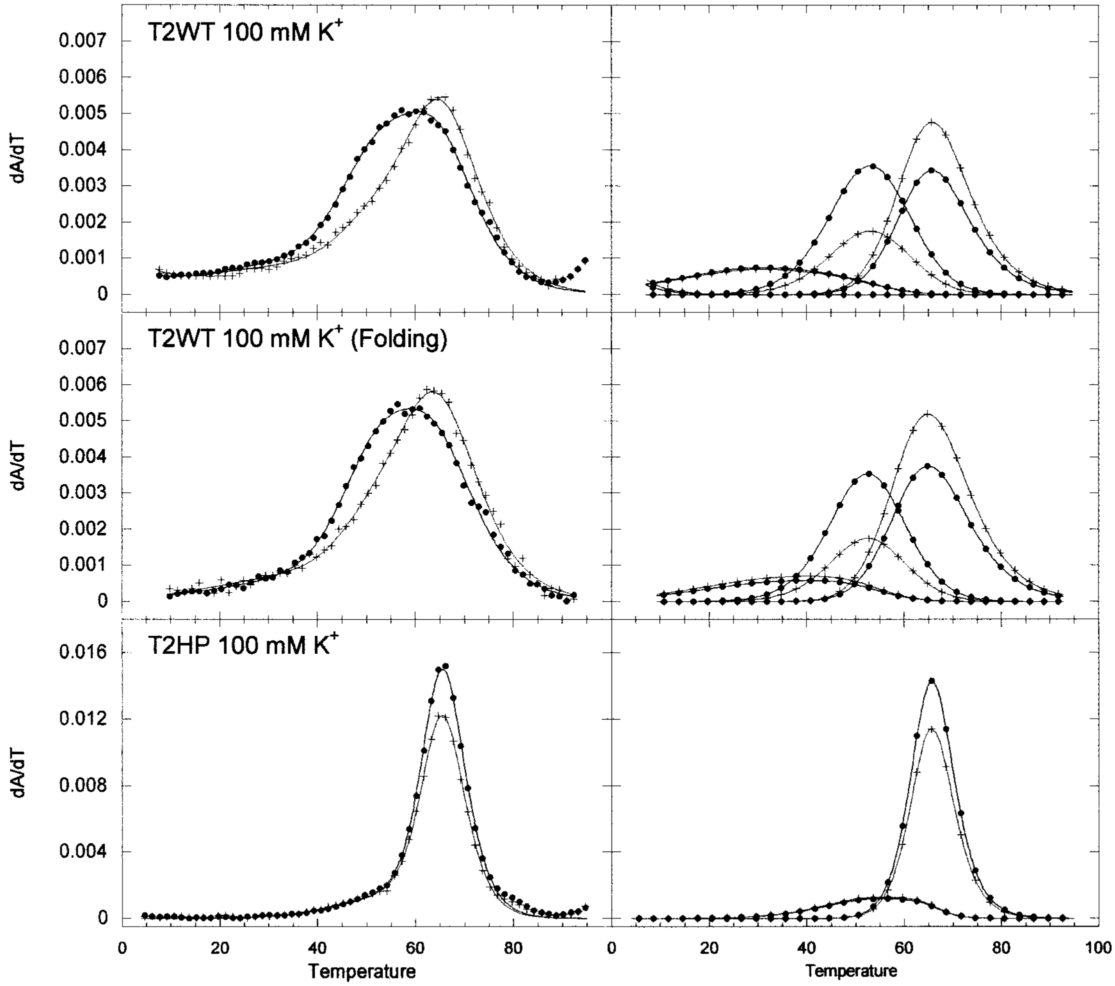

FIGURE 2: Melting profiles for the T2 WT pseudoknot and the T2 stem 2 hairpin (T2HP) in the absence of added Mg^{2+}. The center profile illustrates the thermodynamic reversibility of the system. The left side shows composite fits superimposed on every fifth point of the experimental data. The right side shows the individual transitions of the composite fit. Black (●) and gray-scale (+) correspond to ∂A/∂T monitored at 260 and 280 nm, respectively.

Table 1: Thermodynamic Parameters Obtained for the Unfolding of the T2 Pseudoknot (WT) and T2 Stem 2 Hairpin (T2HP) RNAs[a]

RNA	conditions	transition	A_{260}/A_{280}	t_m (°C)	ΔH (kcal mol^{-1})	ΔH_{total}
WT, heating	100 mM K$^+$	1	1.0	31.0	17.0	95
		2	2.0 (1 + 2: 1.6)[b]	52.3	34.4 (1 + 2: 51)	
		3	0.7	66.0	43.2	
WT, cooling	100 mM K$^+$	1	0.9	31.0	12.2	87
		2	2.1 (1 + 2: 1.4)	51.4	34.8 (1 + 2: 47)	
		3	0.7	65.5	40.0	
WT	100 mM K$^+$, 8.0 mM Mg^{2+}	1	1.0	58.0	17.8	121
		2	1.8 (1 + 2: 1.3)	72.9	55.9 (1 + 2: 73.7)	
		3	0.8	81.0	47.7	
WT	1.0 M K$^+$	1	1.0	56.9	15.0	111
		2	1.8 (1 + 2: 1.3)	68.9	47.0 (1 + 2: 62)	
		3	0.7	77.6	49.3	
T2HP	100 mM K$^+$	1	0.9	51.8	30.0	101
		2	1.3	65.4	71.6	
T2HP	100 mM K$^+$, 8.0 mM Mg^{2+}	1	1.1	68.4	25.0	104
		2	1.4	74.8	78.8	

[a] Derived from the four sequential transition fits shown in Figures 2 and 3. [b] 1 + 2 is the arithmetic sum of the amplitude ratio or ΔH obtained for transitions 1 and 2.

major transition, the major transition is characterized by the expected enthalpy, t_m, and hyperchromicity ratio with a A_{260}/A_{280} ratio ≈ 1.3 in light of previous studies on the stem 2 hairpin from the T4 sequence (*20*). On the basis of the amplitude and returned ΔH, the minor transition is attributed to secondary structure associated with the twelve-nucleotide loop in the T2HP RNA; indeed, secondary structure prediction algorithms predict that the loop of the T2 stem 2 hairpin RNA will fold into a 3-base-pair stem that could stack on the existing stem 2 producing an extrahelical bulged G27, fully consistent with the thermodynamic parameters derived for this transition. Two points can be made from these data.

Turner rules (*30*) predict that the 7-base-pair stem 2 will be slightly more stable than the 5-base-pair stem 1; this, in turn, predicts that the partially folded stem 2 hairpin should appear as an intermediate in the unfolding pathway. This behavior is observed in the T4 pseudoknot, which has a less-stable 4-base-pair stem 1 (*20*). However, this prediction is strongly affected by any contributions of noncanonical structure to the energetics of helix−helix and helix−loop interactions, in addition to simple loop-closing penalties associated with the pseudoknot. From simple inspection of the melting profile for stem 2 hairpin RNA, it is clear that the unfolding transition associated with stem 2 of the T2 pseudoknot does not appear as an intermediate in the melting profile. To illustrate, the first major optical transition in the T2 melting profile has an A_{260}/A_{280} ratio of ≈2 with the van't Hoff enthalpy about half the expected value of 76 kcal mol^{-1} for stem 2 unfolding (Table 1). In contrast, the enthalpy and A_{260}/A_{280} ratio determined for the second major transition are similar to those which are predicted from Turner rules and hyperchromicity arguments (*31*) for the unfolding of the stem 1 hairpin. The melting profile of the wild-type T2 pseudoknot in the absence of added salts returns a smaller total van't Hoff enthalpy of unfolding (≈95 kcal mol^{-1}) relative to that predicted from Turner rules (122 kcal mol^{-1}), and the unfolding pathway is not clearly defined by the data.

Magnesium Dependence of the Unfolding of the T2 Pseudoknot. Melting profiles were therefore collected for the wild-type pseudoknot over a wide range of Mg^{2+} (0.1−10 mM) in the presence of fixed monovalent cation (0.10 M K^+) or in the presence of 1.0 M K^+ only. Selected melts are shown in Figure 3, with the thermodynamic parameters summarized in Tables 1 and 2. A plot of the effect of Mg^{2+} concentration on the resolved van't Hoff enthalpy of the first two transitions is shown in Figure 4. The most striking finding from the Mg^{2+} dependence of the melting profiles is that the first major transition sharpens considerably (Figure 3) and returns nearly 2-fold more van't Hoff enthalpy to an average value of 55 ± 3 kcal mol^{-1} at $[Mg^{2+}] \geq 1$ mM. This suggests that the molecule either is only partially folded in low or no magnesium or exhibits significant non-two-state melting behavior at low magnesium (stem 2; see below).[3] In contrast, the returned ΔH for the first broad transition is relatively constant over the same Mg^{2+} concentration range at $\Delta H \approx 18 \pm 3$ kcal mol^{-1}. At high Mg^{2+}, the total van't Hoff enthalpy associated with these two transitions is ∼73 ± 3 kcal mol^{-1}, indistinguishable from the experimentally determined 75 kcal mol^{-1} for the cooperative unfolding of the 7-base-pair stem 2 hairpin (ΔH = 76 kcal mol^{-1} predicted) (Figure 2, Table 1). Strikingly, if the recovered amplitude of the hyperchromicity is summed for these two transitions, the composite A_{260}/A_{280} ratio is 1.4 ± 0.1, identical to that obtained for the stem 2 hairpin (*20*) (Figure 2). Thermodynamic analysis of the second major unfolding transition returns a ΔH of 47 ± 3 kcal mol^{-1} and a A_{260}/A_{280} ratio of 0.7, parameters consistent with the melting of the short 5-base-pair helical stem 1 (ΔH = 46 kcal mol^{-1} predicted). The maximal combined enthalpy of unfolding for these three transitions in the presence of high divalent or trivalent cation concentration is ∼125 kcal mol^{-1}, similar to that predicted from secondary structure alone from Turner rules (Table 2).[4] Interestingly, analysis of T2 melting profiles collected in the presence of high monovalent salt concentration (1.0 M K^+ only) reproducibly yields slightly less total unfolding enthalpy (Table 1, Figure 3) with this loss occurring primarily in transition 2.

Additional effects of magnesium concentration on the thermal unfolding of the wild-type T2 pseudoknot are discussed below.

Thermodynamic Analysis of the Unfolding of Stem Assignment Mutants. Taken collectively, the data above suggest that stem 2 unfolds in two operationally definable steps in the context of the pseudoknot, followed by the unfolding of stem 1. To obtain direct support for this unfolding pathway as well as to gain insight into the complex energetics of this system, we prepared four compensatory base pair substitution mutants (Figure 1A). These are a potentially stabilizing substitution of the U18-A5 base pair in stem 1 with a C18-G5 base pair (C18-G5 RNA), and three substitutions in stem 2, two of which are potentially destabilizing, G14-C29 → A14-U29, one base pair removed from the helical junction, and C10-G33 → A10-U33, one base pair removed from the terminal base pair in stem 2, and one of which is potentially stabilizing, U11-A32 → C11-G32. In addition, previous studies revealed that the 3′ AC single-stranded tail essentially forms a helix cap on stem 2, thereby extending the helical sense of the molecule (*23*, *24*). This cap appears to play a significant role in stabilizing the single-nucleotide loop 1 conformation of the molecule, beyond that anticipated from nearest-neighbor interactions (*20*). Therefore, a Δ3′ cap RNA was prepared to test this in the context of the T2 backbone.

Melting profiles for these RNAs were obtained over the entire range of $[Mg^{2+}]$ from 0 to 10 mM. Representative optical melting profiles are shown for these RNAs compared to wild-type T2 in Figure 5 in the presence of 0.10 M K^+ and 0.5 mM Mg^{2+} with experimental data and composite fits shown as previously described. The parameters derived from these fits are collected in Table 3. The C18-G5 RNA (Figure 5, top panel) gives rise to a melting profile which differs from the wild-type RNA by moving the third transition to a higher t_m, with a corresponding reduction in the A_{260}/A_{280} ratio to 0.54; all other aspects of the profile are nearly identical to that of the wild-type molecule. In addition, the expected increase in ΔH of 2.9 kcal mol^{-1} is also observed. These characteristics are consistent with the stabilization of stem 1 by replacement of a U−A base pair with a C−G base pair. This unambiguously defines the last melting transition as reported on unfolding of helical stem 1.

The melting profiles for A10-U33 and A14-U29 RNAs (Figure 5) are indicative of a major effect on the melting

---

[3] The solution structure of the T2 pseudoknot solved in the absence of divalent cations (Du et al., 1996)[2] provides no evidence for partial unfolding of the molecule under these conditions although detailed structural information outside of the helix−helix junction itself, for example, on potential loop−stem interactions, remains lacking. Preliminary differential scanning calorimetry experiments suggest that slightly less calorimetric enthalpy is recovered in the absence versus in the presence of 10 mM Mg^{2+} (95 vs 120 kcal mol^{-1}, respectively) (P. Nixon and D. Giedroc, unpublished results).

[4] All melting profiles collected at high divalent and multivalent cation concentrations contained an additional low-enthalpy ($\Delta H \approx 20$ kcal mol^{-1}) unfolding transition with a t_m in the 10−20 °C range, far below 37 °C. The transition is largely absent from melts collected in the absence of multivalent ions (cf. Figure 3). The molecular assignment of this transition is unknown but may well correspond to the melting of loop-stem interactions.

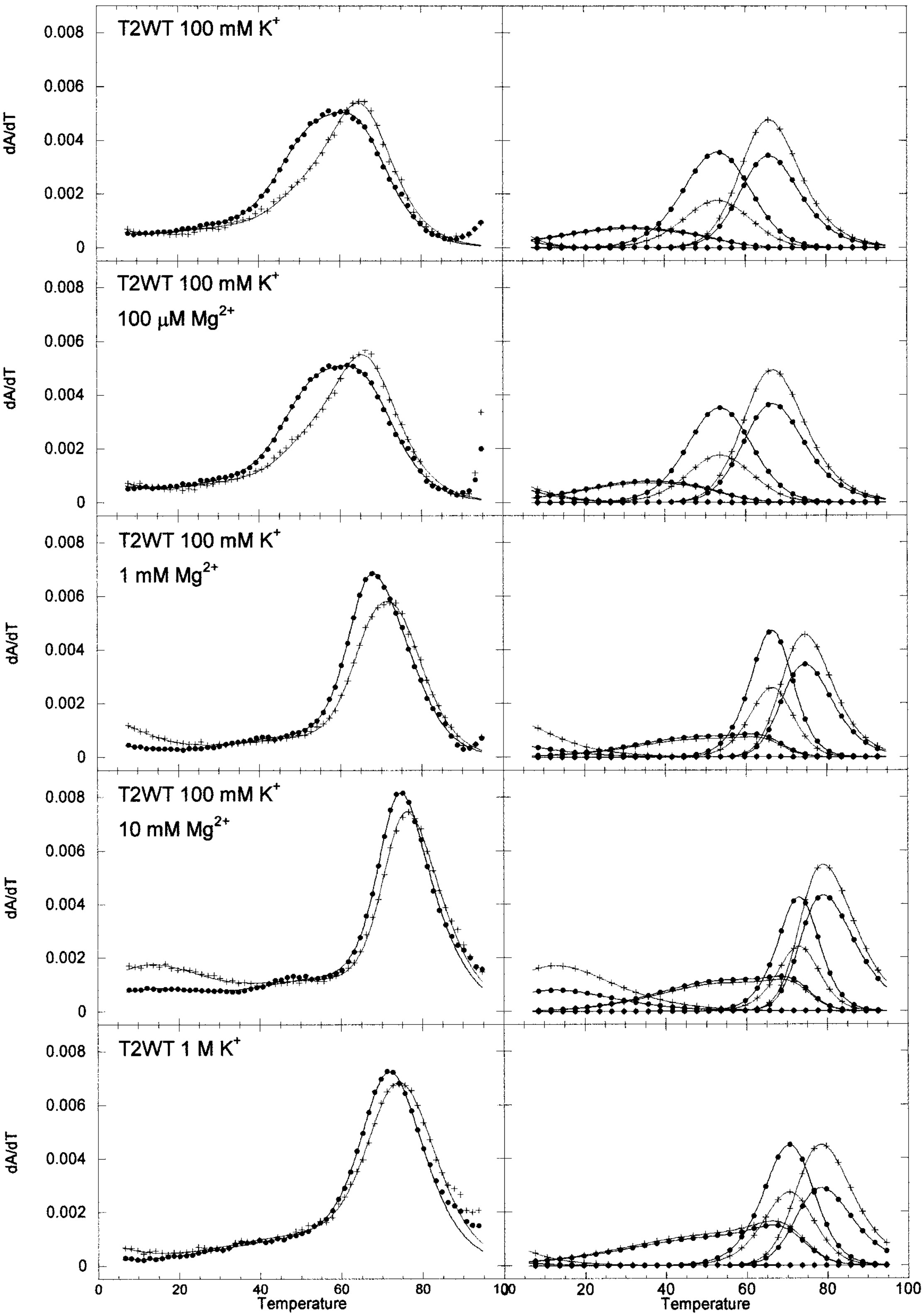

FIGURE 3: $[Mg^{2+}]$ dependence of the melting profile of the T2 WT pseudoknot. Melting profiles are shown in decades of added Mg^{2+} with 0.10 M K^+ in all but the final panel which contains 1.0 M K^+ only: left, composite fits superimposed on the experimental data; right, individual transitions of the composite fit. Black (●) and gray-scale (+) correspond to $\partial A/\partial T$ monitored at 260 and 280 nm, respectively.

transitions 1 and 2, with a correspondingly much smaller effect on transition 3. In particular, introduction of each A−U base pair dramatically increases the A_{260}/A_{280} ratio of transition 2 with a correspondingly smaller effect on transition 1. Turner rules predict that A14-U29 RNA nearest to the junction should be destabilized by 9 kcal mol^{-1} in enthalpy compared to 3 kcal mol^{-1} for the A10-U33 RNA for stem 2 melting. Interestingly, the A14-U29 substitution has the effect of moving some enthalpy from transition 2 to transition 1, relative to the wild-type pseudoknot; this persists over the entire range of $[Mg^{2+}]$ investigated (data not shown) (Table 3).

Table 2: Mg^{2+} Dependence of the Thermodynamics of Unfolding of Wild-Type T2 Pseudoknots at 0.10 M KCl, pH 7.0[a]

$[Mg^{2+}]$ (mM)	transition	A_{260}/A_{280}	t_m (°C)	ΔH (kcal mol^{-1})	ΔH_{pred} (kcal mol^{-1})	ΔH^{total} $(\Delta H_{pred})^{total}$
0	1	1.1	31.0[b]	17.0		
	2	2.0 (1 + 2: 1.6)	52.3	34.4 (1 + 2: 51.4)	76.0	
	3	0.7	66.0	43.2	45.9	95 (122)
0.1	1	1.1	35.0[b]	18.1		
	2	2.0 (1 + 2: 1.6)	52.9	35.7 (1 + 2: 53.8)	76.0	
	3	0.7	67.0	42.2	45.9	96 (122)
0.3	1	1.2	37.0[b]	17.0		
	2	1.9 (1 + 2: 1.6)	57.9	42.4 (1 + 2: 59.4)	76.0	
	3	0.7	69.6	46.1	45.9	106 (122)
1.0	1	1.1	50.1	18.5		
	2	1.8 (1 + 2: 1.5)	65.7	55.9 (1 + 2: 74.4)	76.0	
	3	0.8	75.2	51.8	45.9	126 (122)
2.0	1	1.1	48.5	21.3		
	2	1.7 (1 + 2: 1.5)	69.0	52.3 (1 + 2: 73.6)	76.0	
	3	0.7	77.1	50.8	45.9	124 (122)
3.0	1	1.2	52.9	21.0		
	2	1.6 (1 + 2: 1.4)	70.8	52.5 (1 + 2: 73.5)	76.0	
	3	0.7	79.3	49.0	45.9	123 (122)
5.0	1	1.0	52.8	18.3		
	2	1.6 (1 + 2: 1.3)	71.5	54.7 (1 + 2: 73.0)	76.0	
	3	0.7	79.9	48.3	45.9	121 (122)
10.0	1	1.1	53.5	18.4		
	2	1.8 (1 + 2: 1.4)	72.7	56.3 (1 + 2: 74.7)	76.0	
	3	0.8	80.0	45.0	45.9	120 (122)

[a] Derived from the four sequential transition fits shown in Figures 2-3, 5. Parameters derived from the 0.5 and 8.0 mM Mg^{2+} optical melting profiles are presented in Tables 3 and 1, respectively. [b] Upper limit of this parameter value reached in the curve fitting analysis.

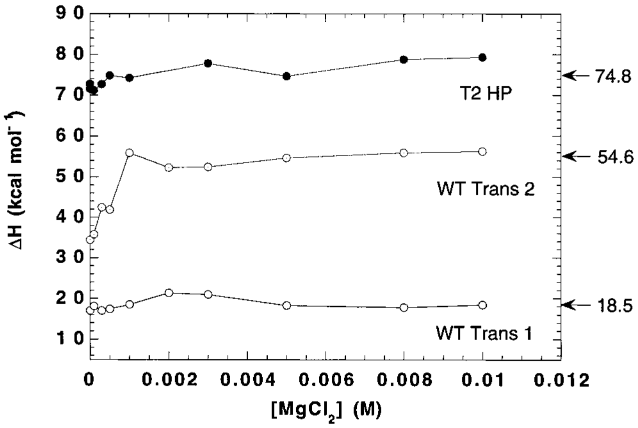

FIGURE 4: The effect of Mg^{2+} on the van't Hoff enthalpy of pseudoknot transitions 1 and 2 for T2 WT compared to the total van't Hoff enthalpy obtained for the melting of the stem 2 within the T2 HP RNA.

The melting profile for the stabilizing stem 2 substitution, C11-G32 RNA, is indicative of moving much of the amplitude from transitions 1 and 2 into the major transition 3, exactly as qualitatively predicted (data not shown). Although a quantitative analysis of these melting profiles was unsuccessful due to strongly overlapping transitions, the total van't Hoff enthalpy derived from a three-transition analysis is 80 kcal mol^{-1} at 0.5 mM Mg^{2+} but 118 kcal mol^{-1} at $[Mg^{2+}] \geq 3$ mM, close to that predicted from Turner rules (129 kcal mol^{-1}) (Table 3). Melting profiles obtained for another stabilizing stem 2 G−C substitution mutant, G15-C28 RNA, were qualitatively identical to that of the C11-G32 RNA (data not shown).

The melting profile for the 3′ cap deletion (Δ3′ cap RNA) is qualitatively like that of the wild-type RNA (Figure 5), except that the ΔH values of unfolding of transitions 1 and 2 are significantly smaller with, again, essentially no effect on transition 3 (Table 3). Turner rules predict that stem 2 should be destabilized by 9 kcal mol^{-1} in enthalpy upon removal of the single-stranded tail; this is approximately the $\Delta(\Delta H)$ for transition 2 (Table 3), thermodynamic evidence that the 3′ tail is stacked against the base of the stem 2 helix.

These thermodynamic data are summarized as $\Delta(\Delta H)$ and $\Delta(\Delta G°)$ (37 °C) values relative to the wild-type T2 RNA in Figure 6. Analysis of these data for all mutations which are predicted to destabilize stem 2 (A10-U33, A14-U29, and Δ3′ cap RNAs) reveals that the magnitude of $\Delta(\Delta H)$ varies most dramatically for melting transitions 1 and 2, with a comparably negligible effect on transition 3. This is more striking in the $\Delta(\Delta G°)$ (37 °C) values. In contrast, the major effect of the stabilizing stem 1 substitution (C18-G5) is to increase the enthalpy and free energy of unfolding of transition 3, with correspondingly smaller perturbations in the other two unfolding transitions.

Interestingly, for all three stem substitution mutants, the $\Delta(\Delta G°)$ (37 °C) values are significantly larger for the two destabilizing mutants and smaller for the C18-G5 stabilizing mutant than those predicted on the basis of Turner rules alone (numerical values in brackets). For example, the $\Delta(\Delta G°)$ (37 °C) for the A14-U29 mutant is −4.2 kcal mol^{-1}, the majority of which falls in transitions 1 and 2, with the predicted $\Delta(\Delta G°)$ (37 °C) being −2.1 kcal mol^{-1}. Similarly, for the A10-U33 RNA, the $\Delta(\Delta G°)$ (37 °C) is −3.3 kcal mol^{-1} with the predicted $\Delta(\Delta G°)$ (37 °C) being −1.9 kcal mol^{-1}. Likewise, the $\Delta(\Delta G°)$ (37 °C) experimentally determined for the C18-G5 RNA is less positive than that predicted [$\Delta(\Delta G°)$ $(37\ °C)_{pred} = +1.9$ kcal mol^{-1}].

Finally, deletion of the 3′ ss helical cap at the base of stem 2 not only gives rise to expected nearest-neighbor destabilization of melting transition 2 [$\Delta(\Delta H) = -9$ kcal mol^{-1} (−9 kcal mol^{-1} expected); $\Delta(\Delta G°) \approx -2.1$ kcal mol^{-1} (−1.7 kcal mol^{-1} expected)] but also gives rise to enthal-

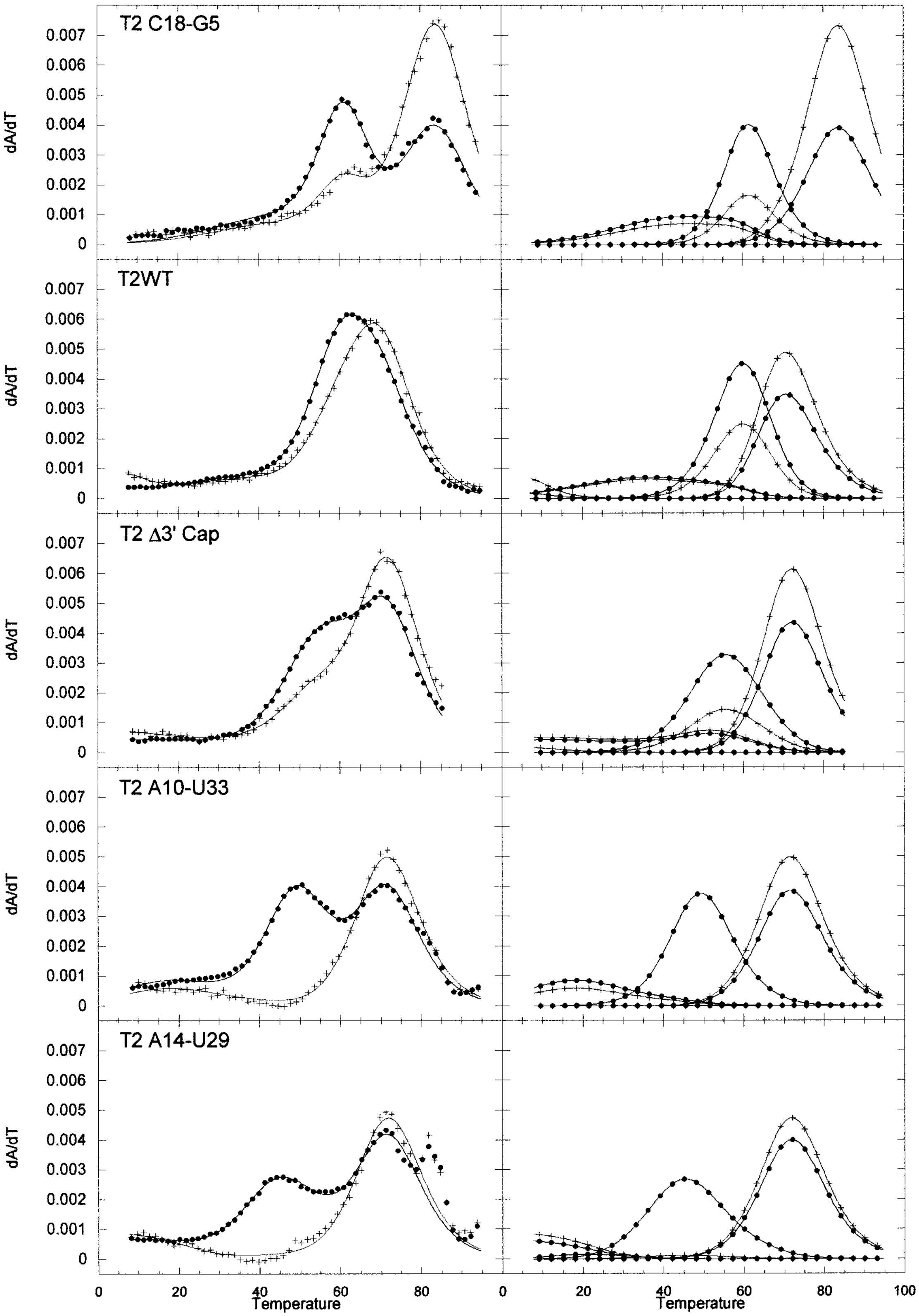

FIGURE 5: Representative melting profiles for stem substitution and Δ3′ cap mutant RNAs collected in 500 μM Mg^{2+}, 0.10 M K^{+}: left, composite fits superimposed on the experimental data; right, individual transitions of the composite fit. Black (●) and gray-scale (+) correspond to $\partial A/\partial T$ monitored at 260 and 280 nm, respectively.

pically derived non-nearest-neighbor destabilization of transition 1 [$\Delta(\Delta H) = -7$ kcal mol^{-1}; $\Delta(\Delta G°) \approx -0.5$ kcal mol^{-1}] (see also ref 20).

Our thermodynamic analysis of the unfolding of the wild-type T2 pseudoknotted RNA and compensatory base pair substitution mutants is consistent with the unfolding (folding) pathway shown in Figure 7. From the magnitude of the maximum recovered enthalpy of transitions 1 and 2 and the thermodynamic behavior of the stem substitution mutants, we conclude that the molecule is characterized by three sequential unfolding transitions as predicted from preliminary studies (*23*). The unfolding of helical stem 2 exhibits

Table 3: Thermodynamic Parameters for the Unfolding of Mutant T2 Pseudoknots at 0.10 M KCl, 0.5 mM Mg^{2+}, pH 7.0[a]

RNA	transition	A_{260}/A_{280}	t_m (°C)	ΔH (kcal mol^{-1})	ΔH_{pred} (kcal mol^{-1})	ΔH^{total} $(\Delta H_{pred})^{total}$
WT	1	1.1	37.0	17.4		
	2	1.8 (1 + 2: 1.5)	59.4	41.9 (1 + 2: 59.3)	76.0	
	3	0.7	71.1	44.2	45.9	104 (122)
A10-U33	1	1.4	17.6	18.4		
	2	All 260 (1 + 2: 5.1)	49.4	39.0 (1 + 2: 57.4)	73.2	
	3	0.8	72.0	44.1	45.9	102 (119)
A14-U29	1	All 260	20.9	25.7		
	2	22 (1 + 2: 23)	45.9	30.9 (1 + 2: 56.6)	67.0	
	3	0.8	72.2	43.4	45.9	100 (113)
C18-G5	1	1.3	44.3	19.2		
	2	2.4 (1 + 2: 1.2)	60.9	49.4 (1 + 2: 68.6)	76.0	
	3	0.5	84.1	48.0	48.8	117 (125)
C11-G32	1	0.9	64.2	21.5	83.0	
	2	0.9	72.8	58.4	45.9	80 (129)
Δ3′ cap	1	0.8	36.6	7.2		
	2	2.3 (1 + 2: 1.5)	53.0	33.2 (1 + 2: 40.4)	67.0	
	3	0.7	72.3	45.7	45.9	86 (113)

[a] Derived from the four sequential transition fits shown in Figure 5.

extreme non-two-state melting behavior and can be modeled as occurring in two distinct steps. On the basis of the maximum recovered enthalpy in transitions 1 and 2 (18 and 55 kcal mol^{-1}, respectively), the first step might correspond to an unfolding of the junction region including any tertiary or non-Watson−Crick structure, the coaxial stack,[1] and the A15-U28 base pair ($\Delta H_{pred} = 21$ kcal mol^{-1}) with the remainder of stem 2 melting next ($\Delta H_{pred} = 55$ kcal mol^{-1}). The third unfolding transition corresponds to the melting of the shorter stem 1. Furthermore, substitution of the G14-C29 base pair one base pair removed from the junction appears more enthalpically destabilizing than substitution of the C10-G33 base pair near the base of stem 2 or deletion of the 3′ single-stranded cap altogether. This suggests that the junction region in the T2 pseudoknot is considerably weaker relative to the immediately adjacent helical regions of the pseudoknot.

Effect of Magnesium Ions on the Stability of Wild-Type and Mutant T2 RNAs. The data presented above are consistent with the temperature-induced unfolding pathway for the T2 pseudoknot proceeding via three optically definable steps containing two intermediates, termed J (unfolded junction) and S1 (stem 1 hairpin), from the folded (F) to the fully unfolded (U) form of the molecule:

$$F \Leftrightarrow J \Leftrightarrow S1 \Leftrightarrow U$$

Since complete melting profiles have been collected for all RNAs over a wide range of [Mg^{2+}], the complete [Mg^{2+}] dependence of the three equilibrium constants which govern the unfolding pathway for these RNAs can be obtained (see eqs 3−5 in Materials and Methods).

Figure 8 presents a fractional species population analysis of the unfolding of the wild-type T2 RNA at a few select [Mg^{2+}] from 0.1 to 10.0 mM. This analysis of the T2 RNA has two clear implications. One is that the partially unfolded J form of the molecule is significantly populated at physiological temperatures over a wide range of Mg^{2+} concentration. This suggests that the helical junction region of the T2 pseudoknot is rather weak even at high concentrations of divalent ions and may well be partially unfolded at moderate temperatures (20−30 °C) in the absence of Mg^{2+} and 0.10 M K^+. Second, the effect of increasing [Mg^{2+}] on the species population of conformers is *not* to significantly change the fractional representation of individual species at high versus low [Mg^{2+}] at any one temperature, that is, to make the unfolding more cooperative, which would be expected if magnesium was specifically stabilizing a true tertiary structure (*14*). This strongly suggests that, although magnesium dramatically stabilizes the folded conformation of the molecule and, in this case, induces a significant and specific increase in the returned van't Hoff enthalpy of transition 2, it does so in a relatively nonspecific way.[5] The fact that the total van't Hoff enthalpy is identical to that predicted from base stacking alone also suggests that thermodynamically defined high affinity and specific Mg^{2+} ion binding sites in the pseudoknot are not present (*14*, *18*, *26*). Thus, an appropriate model with which to analyze the effects of the [Mg^{2+}] on the individual unfolding steps is a completely nonspecific one, in which every phosphate on the RNA is a potential Mg^{2+} binding site and each Mg^{2+} is capable of interacting with the RNA backbone with an excluded site size of 2 (*18*, *26*, *32*). Although the details of this model may be oversimplified, it is used here to compare the behavior of individual RNAs in order to identify internally consistent trends in the data.

Figure 9 plots $1/t_m$ versus log [Mg^{2+}] for the J → S1 (panel A) and S1 → U (panel B) unfolding transitions for some or all of the RNAs investigated here, compared to that obtained for the unfolding of the T2HP (panel C), all at 0.10 M K^+. Similar plots were constructed for the F → J transition as well (data not shown). The continuous curves drawn through the data are fits to the nonspecific binding model with the magnesium binding affinities (K_i) collected in Table 4 (eq 5). In all cases, the number of phosphates (m) participating in the F → J, J → S1, and S1 → U unfolding transitions for all pseudoknotted RNAs was fixed at 4, 10, and 10 ($m = 14$ for the T2HP RNA), consistent with the unfolding model. Increasing (or decreasing) m by two phosphates in all cases

---

[5] The limitations of the model do not rule out the presence of one or a small number of somewhat higher-affinity Mg^{2+} binding sites in the molecule, which may make large contributions to the stability. In fact, a higher-affinity $Co(NH_3)_6^{3+}$ binding site appears to be localized at or near the C10-G33/U11-A32 base pair step and requires the single loop 1 nucleotide on the pseudoknot to display high affinity (P. Nixon, C. Theimer and D. Giedroc, manuscript in preparation).

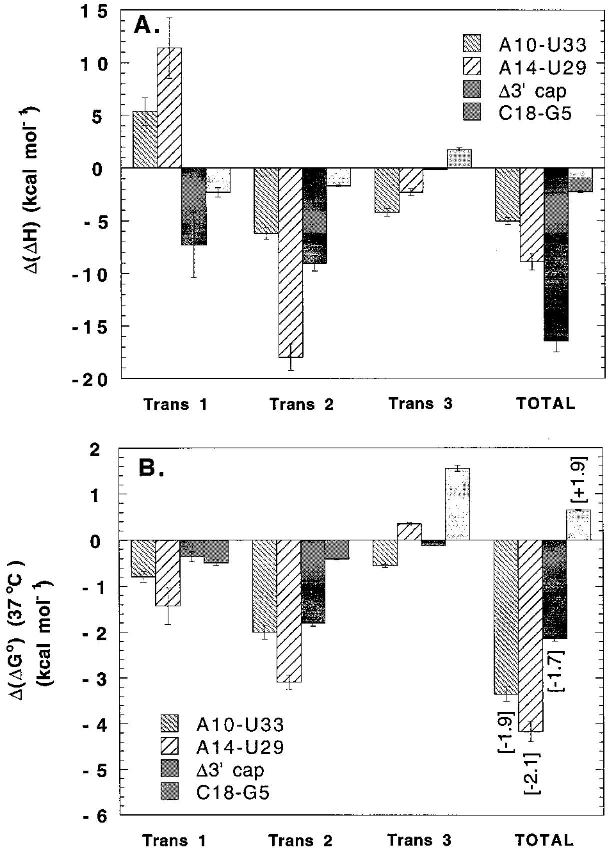

FIGURE 6: A bar graph summary of Δ(Δ*H*) (panel A) and Δ(Δ*G*°) (37 °C) (panel B) values for the stem assignment mutant RNAs relative to wild-type T2 RNA. The values in brackets (panel B) correspond to the Δ(Δ*G*°) (37 °C) predicted from the nearest-neighbor model. The average Δ*H* and Δ*G*° (37 °C) values calculated from the optical melts for wild-type pseudoknot for transitions 1, 2, and 3, respectively, are as follows: $\Delta H = 18$ kcal mol^{-1}, $\Delta G° = 1.0$ kcal mol^{-1}; $\Delta H = 55$ kcal mol^{-1}, $\Delta G° = 5.7$ kcal mol^{-1}; and $\Delta H = 47$ kcal mol^{-1}, $\Delta G° = 5.8$ kcal mol^{-1}. Summing these values gives a total denaturational Δ*H* and Δ*G*° (37 °C) of 120 and 12.5 kcal mol^{-1}, respectively. To calculate Δ*H*, the mean and standard deviations over all [Mg^{2+}] are shown for each transition in each RNA, provided there was no evidence of a systematic trend in these values. If there was, the mean values were taken at a [Mg^{2+}] ≥ 1.0 mM (e.g., stem 2). To calculate Δ*G*° (37 °C), only melts collected at [Mg^{2+}] ≥ 5.0 mM were considered.

had no effect on the quality of the fit while still returning reasonable values for K_u (*26*, *32*); decreasing or increasing *m* by more than this returns K_u values that are too small or too large, respectively, at 0.10 M K$^+$, based on model studies (*32*).

Analysis of the unfolding data for the T2HP returns K_f and K_u values which are in agreement with model studies (*32*) and previous studies with several known RNA hairpins (*26*). They differ by approximately a factor of 2, with K_u in the 200−300 M^{-1} range. Interestingly, analysis of the [Mg^{2+}] dependence of the unfolding transitions for the wild-type T2 RNA leads to essentially the same qualitative conclusion for only the last unfolding step, S1 → U, or melting of a 5-base-pair stem 1 hairpin, with K_f and K_u perhaps only marginally higher than for T2HP, but which differ from one another by the same factor of ~2 (Table 4). This appears to be true for the S1 → U step in all RNAs. In contrast, analyses of the [Mg^{2+}] dependence of the F → J and J → S1 steps for the wild-type, A10-U33, and C18-G5 RNAs are indistinguishable within experimental error, with K_f approximately 3−4-fold larger than K_u or about 2-fold larger than K_f for the S1 → U unfolding step. These findings suggest that the fully folded and partially folded J intermediates bind Mg^{2+} with marginally higher average affinity than a typical hairpin RNA structure. This leads to a significantly larger extent of binding of Mg^{2+} at a constant [Mg^{2+}], with a correspondingly larger number of these ions released upon unfolding (Table 4). Interestingly, analysis of the [Mg^{2+}] dependence of the t_m for the two mutant RNAs which significantly destabilize the helix−helix junction (A14-U29 RNA) or the base of stem 2 and perhaps the junction (Δ3′ cap RNA) reveals K_f and K_u values for the J → S1 step more similar to hairpin unfolding than for the J → S1 step form of the pseudoknot. This results in fewer ions being bound by the folded and partially folded J intermediate, with a correspondingly smaller number released upon unfolding (Table 4). This suggests that whatever is responsible for the higher Mg^{2+} affinity in the wild-type pseudoknot may be effectively lost in these two mutants. Similar findings characterize the globally destabilized A8 → U8 substitution mutant of the T2 RNA but not other weakly destabilized mutants.[1]

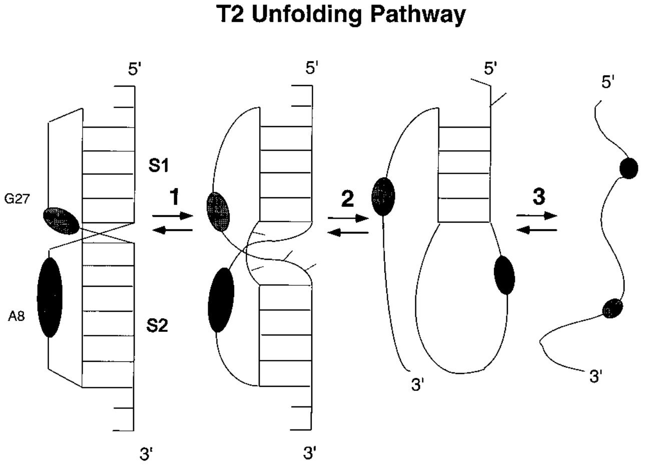

FIGURE 7: The proposed unfolding pathway of the T2 pseudoknot based on the sequential two-state, dual-wavelength unfolding analysis of the wild-type and stem assignment mutants.

DISCUSSION

As an H-type RNA pseudoknot is simply composed of two helical stems connected by two nonequivalent loops, its total folding energy must derive from the stems, which are well-approximated by the nearest-neighbor base-stacking enthalpies and entropies (Turner rules) (*30*): a coupling energy term, composed of the helical stacking junction enthalpy and entropy and loop-closing entropies; and, superimposed on this, any additional non-Watson−Crick loop−stem interactions. To deconvolute the energetics of even this simple RNA conformation, and therefore thermodynamically define the importance of potential stabilizing interactions in this conformation, we must first determine the unfolding pathway.

In this paper, the unfolding (folding) pathway of the bacteriophage T2 autoregulatory gene *32* mRNA pseudoknot has been determined through a thermodynamic characterization of the unfolding of wild-type RNA and compensatory

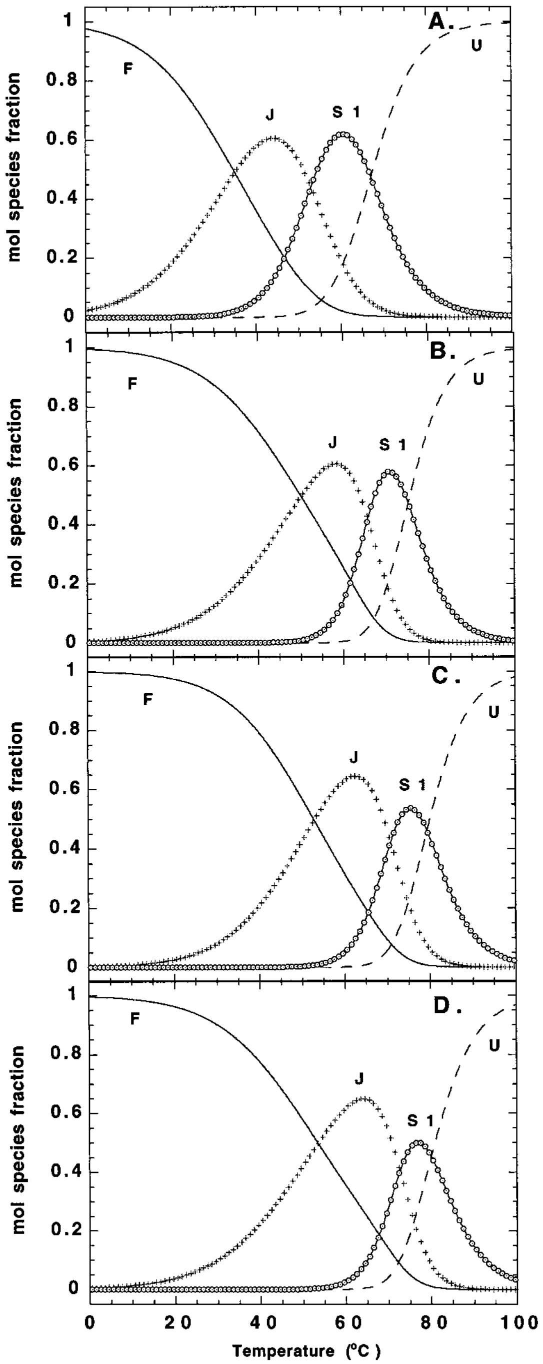

FIGURE 8: Fractional species population analysis of the thermal unfolding of the T2 WT RNA as a function of Mg^{2+} concentration (only select concentrations are shown) derived from the parameters obtained from the analysis of the melting profiles (cf. Figure 3): A, 0.1 mM Mg^{2+}; B, 1.0 mM Mg^{2+}; C, 3.0 mM Mg^{2+}; D, 10.0 mM Mg^{2+}. F stands for folded RNA; J, unfolded junction intermediate; S1, stem 1 hairpin intermediate; and U, unfolded RNA. See text for details.

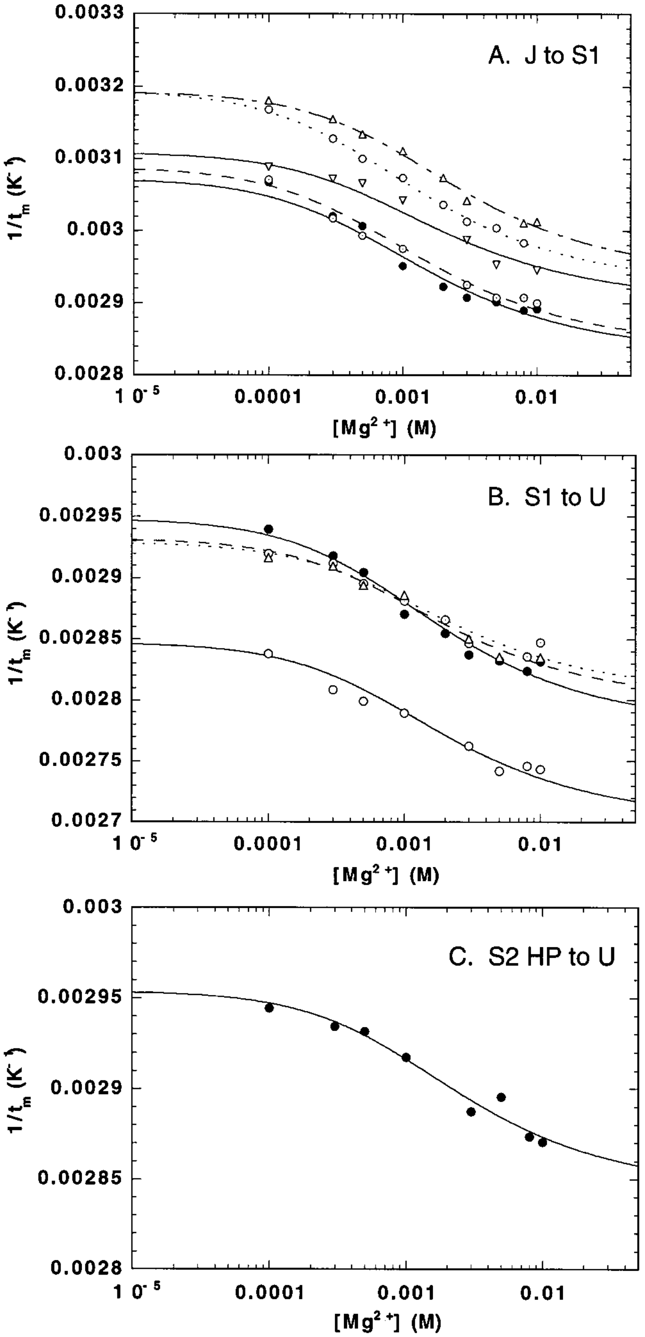

FIGURE 9: Effect of [Mg^{2+}] on the t_m for individual unfolding transitions in different RNAs. (A) Dependence of $1/t_m$ for the J → S1 transition for T2 WT (●), C18-G5 (⊙), Δ3′ cap (▽), A10-U33 (○), and A14-U29 (△) RNAs. (B) Dependence of $1/t_m$ for the S1 → U unfolding step for T2 WT (●), C18-G5 (○), Δ3′ cap (△), and A14-U29 (⊙) RNAs. (C) Dependence of $1/t_m$ for the unfolding of T2 HP RNA (●, major transition). The continuous curves through each data set represent nonlinear least-squares fits to eq 5 with the parameters shown in Table 4. Note that the upper position of the curve is defined by t_m in the absence of added [Mg^{2+}].

base pair substitution mutants (cf. Figure 7):

$$F \Leftrightarrow J \Leftrightarrow S1 \Leftrightarrow U$$

This unfolding pathway returns for the wild-type RNA, at moderate concentrations of divalent cations or in the presence of 1 M monovalent salt, sufficient van't Hoff enthalpy to account for all or nearly all of the known secondary structure in the molecule (122 kcal mol^{-1}), consistent with previous studies (*18*, *20*). Differential scanning calorimetry carried out at 10 mM Mg^{2+} returns the same amount of total calorimetric enthalpy.[3] Only in the presence of high Mg^{2+} is significant additional enthalpy recovered in a low-temperature (t_m below 20 °C), low-enthalpy transition (10−20 kcal mol^{-1})[4] (Figure 3). Low concentrations of $Co(NH_3)_6^{3+}$ also give rise to this transition (data not shown), but it is largely absent in the presence of 1.0 M K^+ (Figure 5), with or without a few millimolar magnesium. This

Table 4: Magnesium-Binding Affinities (K_i) and Extents of Magnesium Binding (ν_i) to various forms of the pseudoknotted T2 RNAs[a]

Magnesium-Binding Affinities (M^{-1})

	$F \rightarrow J^b$		$F \rightarrow J^b$		$F \rightarrow J^b$	
	K_f	K_u	K_f	K_u	K_f	K_u
WT	1200 (±370)	240 (±110)	1100 (±230)	290 (±80)	650 (±130)	290^e
A10-U33	nd	nd	1200 (±80)	310 (±30)	570 (±100)	290^e
A14-U29	nd	nd	520 (±60)	200 (±30)	600 (±150)	350 (±150)
C18-G5	920 (±80)	290^e	1100 (±30)	290^e	600 (±50)	290^e
Δ3′ cap	730 (±220)	240^e	420 (±70)	160 (±40)	580 (±120)	310 (±70)
	$S2 \rightarrow U^f$					
T2HP	440 (±120)	240 (±80)				

Extent of Mg^{2+} Binding (ν_i) at 0.8 mM Mg^{2+}

	$F \rightarrow J^b$		$J \rightarrow S1^c$		$S1 \rightarrow U^d$				
RNA	ν_f	ν_u	$\Delta\nu$	ν_f	ν_u	$\Delta\nu$	ν_f	ν_u	$\Delta\nu$
WT	1.1	0.5	0.6	2.7	1.4	1.3	2.2	1.4	0.8
A10-U33	nd	nd	nd	2.7	1.4	1.3	2.0	1.4	0.6
A14-U29	nd	nd	nd[g]	1.9	1.1	0.8	2.1	1.5	0.6
C18-G5	1.0	0.6	0.4	2.7	1.4	1.3	2.1	1.4	0.7
Δ3′ cap	0.9	0.5	0.4	1.7	0.9	0.8	2.1		
	$S2 \rightarrow U^f$								
T2HP	2.5	1.8	0.7						

[a] Resolved at (0.10 M NaCl) from nonlinear least-squares fits to data like that shown in Figure 9 using eq 3. [b] $m = 4$ phosphates (see eq 3). [c] $m = 10$. [d] $m = 10$. [e] Fixed during the optimization to K_u resolved for the wild-type RNA to facilitate comparison; if K_u and K_f were allowed to vary during the optimization, K_u and K_f were up to ~30% higher, with no effect on $\Delta\nu$. [f] $m=14$ phosphates. [g] nd, not determined.

transition could be attributed to very weak loop 2-stem 1 interactions, although we have no direct evidence for this. Given its low stability and lack of formation at 37 °C, it was not considered further. We therefore conclude that if any loop−stem interactions exist in the structure of the molecule, they do not contribute greatly (probably less than 10 kcal mol^{-1}) to the overall enthalpy term of the free energy of stabilization. This is in contrast to the previous studies of more complex RNAs, including transfer RNA (*25*, *33*), an *Escherichia coli* ribosomal RNA (*16*), and double-pseudoknotted α-mRNA (*17*), in which unfolding enthalpy in excess of 30−40 kcal mol^{-1} could be assignable to the formation of tertiary structure.

It is important to point out that optically defined unfolding "steps" identifiable from a deconvolution of the melting profiles need not necessarily correspond to the formation of physically meaningful, partially folded structural intermediates (cf. Figure 7). In particular, we have no direct structural data that defines to what extent the helical junction is unfolded in the J intermediate. A previous analysis of the temperature dependence of the imino proton spectrum of the T2 pseudoknot in the absence of Mg^{2+}, however, revealed that the imino protons at the junction were in the first group to undergo rapid exchange with solvent upon raising the temperature (*23*). These data and data presented here raise the point that approximation of the unfolding of stem 2 by two sequential two-state transitions may be more of an operational definition of the unfolding pathway; in the extreme case, stem 2 may melt in such a way that no single molecular species predominates during unfolding of the pseudoknot, unlike that shown in Figures 7 and 8. If this were the case, then the free-energy changes calculated for each unfolding transition, and thus the total unfolding free energy of the molecule, may be slightly underestimated, since our free-energy calculations invoke a model (van't Hoff)-dependent interpretation of the energetics. In any case, the two transitions (1 and 2) are interdependent because they are not independent unfolding events; they are reporting on the unfolding of *one* secondary structural unit (helix 2) and thus there is likely to be residual cooperativity or coupling of the unfolding of various parts of the helix.

From the wild-type and mutant RNAs characterized here, we cannot determine if this unfolding pathway is an obligatory one. In other words, would the simultaneous introduction of one or several mutations which destabilize stem 1 and/or strongly stabilize stem 2 significantly alter the unfolding pathway such that stem 1 melts first? An obligatory unfolding pathway is the hallmark of the influence of thermodynamically defined tertiary structure in a folded RNA, in which a set of interactions (outside of Watson−Crick base pairing) must unfold before any subsequent unfolding of the secondary structure (*15*). We suggest that the unfolding pathway in these simple molecules is not an obligatory one, but follows, for the most part, from the relative stability of the two component stems (cf. ref *18*). For example, the T2 and T4 pseudoknots conserve the last nucleotide (G27) in loop 2, the base pairs which make up the helical junction and all of stem 2, as well as the single adenosine in loop 1 (Figure 1A). Stem 1 is one base pair shorter in T4 and has a compensatory decrease in the size of loop 2 (5 vs 7 nucleotides). In this molecule, the unfolding pathway proceeds (*20*)

$$F \Leftrightarrow S2 \Leftrightarrow U$$

exactly in accordance with predictions of the relative stabilities of the two stems, but in contrast to that of T2.

Mg^{2+} ions strongly stabilize the T2 pseudoknot against thermal denaturation, an effect that is largely duplicated by a high concentration of monovalent K^+ ions (Table 1, Figure 3). This result itself makes it unlikely that there is(are) a site-specific Mg^{2+} site(s) on the pseudoknot which is linked to its stabilization (*26*). There are two common ways to model the effect of Mg^{2+} on the stability or t_m of an RNA unfolding transition which can be used to estimate the net number of Mg^{2+} ions displaced on unfolding or $\Delta\nu$ (*18*, *26*). These generally involve linear or nonlinear fits to the $1/t_m$ versus log [Mg^{2+}] data generally appropriate for analysis using a site-specific or nonspecific Mg^{2+} binding model, respectively (*26*). The $1/t_m$ versus log [Mg^{2+}] plots (cf. Figure 9) will be linear only when the folded form has a measurable affinity and the unfolded form has a negligible affinity for the metal ion, behavior consistent with a specific site(s); the slope of such a plot is determined by $\Delta\nu$ and ΔH (*22*). Note that, even in this case, the extent of downward curvature in the $1/t_m$ versus log [Mg^{2+}] plots at low [Mg^{2+}] is dictated by the affinity of the folded form for Mg^{2+}; this portion of the curve is defined by the t_m in the absence of Mg^{2+}. The fact that all plots in Figure 9 have an apparent plateau at low [Mg^{2+}] requires that $1/K_f$ be in the low millimolar range, certainly not that large and in fact comparable to other determinations of the affinity of Mg^{2+} for simple folded RNAs in 0.10 M K^+ (*18*). In contrast, if the unfolded RNA has a significant affinity for Mg^{2+} ions (K_u) that is more similar than different to K_f, the $1/t_m$ versus log [Mg^{2+}] plots will "flatten out" at high [Mg^{2+}] as well, since differential association of Mg^{2+} by each form of the RNA participating in the unfolding transition will incrementally decrease as the [Mg^{2+}] exceeds the reciprocal of both K_i values (*26*).

Since these features qualitatively describe the stabilizing effect of magnesium concentration on the t_m for each unfolding transition quite well (Figure 9), we have analyzed the [Mg^{2+}] dependence of the t_m for individual unfolding steps in the T2 RNA according to a nonspecific, delocalized binding model in which both the folded and unfolded conformations of the RNA or RNA intermediates have significant affinity for Mg^{2+}.[6] An analysis of the [Mg^{2+}] dependence of the stability of a translational read-through pseudoknot using this model also appeared to model the stabilizing effect of Mg^{2+} ions quite well (*18*). Evidence is presented here that both fully folded pseudoknotted and partially folded J intermediate bind Mg^{2+} with a significantly higher affinity than does the partially folded S1 hairpin or other hairpins (e.g., T2HP) (Table 4). As a result of this, the pseudoknot sequesters more Mg^{2+} ions than a similarly sized RNA hairpin, a larger fraction of which are released into bulk solution upon unfolding. The limitations of the nonspecific binding model do not allow us to ascertain if any significantly higher-affinity Mg^{2+} sites exist on the molecule. For example, an average affinity (K_f) perhaps ~2-fold larger for the J conformation of the pseudoknot relative to K_f for an RNA hairpin means that of the nearly three Mg^{2+} ions which are bound to the region of J which participate in the J → S1 unfolding transition at 0.8 mM Mg^{2+} (Table 4), one ion may have a slightly higher affinity, with the other sites behaving as essentially hairpin-type sites. Attempts to fit these data with a model which explicitly considers two classes of "nonspecific" sites (*18*) were unsuccessful due to the fact that the system is strongly underdetermined (data not shown); however, the affinity of such a "stronger" site cannot be more than 2-fold greater, given the small number of ions participating in the transition. We do in fact have NMR evidence that $Co(NH_3)_6^{3+}$ may bind to a "site" preferentially near the base of stem 2 of the pseudoknot.[5] In any case, the data in Table 4 suggest the pseudoknot binds as many as 5−6 Mg^{2+} ions at 0.8 mM Mg^{2+} at 0.10 M K^+, with as many as 2−3 of these ions released upon unfolding (Table 4).

Interestingly, investigation of the magnesium ion concentration dependence of unfolding of the A14-U29 and Δ3′ cap RNAs suggests that these molecules, even in the partially folded J form, sequester fewer divalent ions at some nominal [Mg^{2+}] than do wild-type and other RNAs.[6] The molecular origin of either of these effects is unknown and is not necessarily the same in both cases; however, each could be entirely explained by a small change in the negative charge density in a subtly altered helix−helix junction or on an alteration of the Mg^{2+} binding properties of the base of stem 2, or simply on nonspecific end effects (*32*). NMR experiments may be required to distinguish among these possibilities.

Our data show that the helical junction region of the pseudoknot melts first, in strong contrast to predictions from secondary structural stabilities and previous studies of other RNA pseudoknots (*18*, *20*). What is the molecular origin of this relatively weak helical junction region in the T2 pseudoknot? One possibility is that the full extent of base stacking at the junction itself is not fully realized, which would substantially weaken the interface. In our previous studies of the T4 pseudoknot, introduction of potentially stabilizing or destabilizing base pair substitutions on either side of the junction was not stabilizing or destabilizing to the full extent predicted from the nearest-neighbor model studies (*20*). This might suggest a somewhat structurally altered junction region. Indeed, NMR structural studies suggest that the base pair step at the helix junction is overrotated by 18° which helps to remove close phosphate−phosphate approach in this region (*24*). Another factor that influences the global stability of the molecule by specifically affecting the F → J and J → S1 unfolding steps is the extent to which the pseudoknot loops are destabilizing. Pseudoknot loop-closing energies have not been tabulated due to the lack of a model system in which to make these measurements, although some experiments have been done in this area (*34*). Our previous work on the T4 pseudoknot suggests that the total (loop 1 + loop 2) loop-closing energy is unlikely to be greater than 5−6 kcal mol^{-1} in that system, or roughly consistent with hairpin loop energies (*20*). If one assumes that base-stacking entropies are, like base-stacking enthalpies, comparable to that predicted from Turner rules (Tables 1−3), a folding free energy at 37 °C of −12.5 kcal mol^{-1} for the T2 pseudoknot (Figure 6) requires a total loop-closing energy of nearly 9 kcal mol^{-1}, or slightly larger than that for the T4 pseudoknot. Since loop 1 and the junction region are identical in the T4 and T2 pseudoknots (Figure 1B), our studies suggest that closing a 4-base-pair helical stem 1 with a 5-nucleotide loop 2 (as in T4) is *less* destabilizing than closing a 5-base-pair stem 1 with a 7-nucleotide loop 2 (as in T2). It is not known to what extent nucleotides in loop 2 interact with functional groups in the minor groove of stem

---

[6] Analysis of the [Mg^{2+}] dependence of the t_m for all RNAs studied here with the "site"-binding or linear model (cf. ref *22*) leads qualitatively to the same conclusions reached with the nonspecific binding model concerning both the relative magnitudes of $\Delta\nu$ for the J → S1 and S1 → U transitions, as well as the specifically slightly smaller $\Delta\nu$ for the J → S1 transition for the A14-U29 and Δ3′ cap RNAs (Table 4). It cannot provide an estimate of K_i.

1, which would further increase the entropic penalty for loop closure, since these interactions, if they occur, are clearly not greatly stabilizing. Studies to be reported elsewhere[1] systematically investigate the effects that substitution of loop nucleotides have on the stability of the molecule, focusing in particular on the single adenylate residue in loop 1 (A8) as well as the 3′ nucleotide in loop 2 (G27), which is closest to the junction region (Figure 1B) (*20*).

ACKNOWLEDGMENT

We thank Mr. Jon Christopher for the program t-melt (*20*) and for help in generating Figure 1B. This work was performed in partial fulfillment of the requirements for the Ph.D. degree at Texas A&M University (P.L.N.).

REFERENCES

1. Cate, J. H., Gooding, A. R., Podell, E., Zhou, K., Golden, B. L., Kundrot, C. E., Cech, T. R., and Doudna, J. A. (1996) *Science 273*, 1678−1685.
2. Strobel, S. A., and Doudna, J. A. (1997) *Trends Biochem. Sci. 22*, 262−266.
3. Kolk, M. H., van der Graf, M., Wijmenga, S. S., Pleij, C. W. A., Heus, H. A., and Hilbers, C. W. (1998) *Science 280*, 343−438.
4. Shen, L. X., and Tinoco, I., Jr. (1995) *J. Mol. Biol. 247*, 963−978.
5. Mujeeb, A., Clever, J. L., Billeci, T. M., James, T. L., and Parslow, T. G. (1998*) Nat. Struct. Biol. 5*, 432−435.
6. Philippe, C., Bénard, L., Portier, C., Westhof, E., Ehresmann, B., and Ehresmann, C. (1995) *Nucleic Acids Res. 23*, 18−28.
7. McPheeters, D. S., Stormo, G. D., and Gold, L. (1988) *J. Mol. Biol. 201*, 517−535.
8. Bravo, C., Lescure, F., Laugâa, P., Fourrey, J.-L., and Favre, A. (1996) *Nucleic Acids Res. 24*, 1351−1359.
9. Chen, X., Kang, H., Shen, L. X., Chamorro, M., Varmus, H. E., and Tinoco, I., Jr. (1996) *J. Mol. Biol. 260*, 479−483.
10. Shi, P. Y., Brinton, M. A., Veal, J. M., Zhong, Y. Y., and Wilson, W. D. (1996) *Biochemistry 35*, 4222−4230.
11. McDowell, J. A., He, L., Chen, X., and Turner, D. H. (1997) *Biochemistry 36*, 8030−8038.
12. Kim, J., Walter, A. E., and Turner, D. H. (1996) *Biochemistry 35*, 13753−13761.
13. Morse, S. E., and Draper, D. E. (1995) *Nucleic Acids Res. 23*, 302−306.
14. Turner, D. H. (1996) *Curr. Opin. Struct. Biol. 6*, 299−304.
15. Draper, D. E. (1996) *Trends Biochem. Sci. 21*, 145−149.
16. Laing, L. G., and Draper, D. E. (1994) *J. Mol. Biol. 237*, 560−576.
17. Gluick, T. C., and Draper, D. E. (1994) *J. Mol. Biol. 241*, 246−262.
18. Gluick, T. C., Wills, N. M., Gesteland, R. F., and Draper, D. E. (1997) *Biochemistry 36*, 16173−16186.
19. Michel, F., and Westhof, E. (1996) *Science 273*, 1676−1677.
20. Theimer, C. A., Wang, Y., Hoffman, D. W., Krisch, H. M., and Giedroc, D. P. (1998) *J. Mol. Biol. 279*, 545−564.
21. Shamoo, Y., Tam, A., Konigsberg, W. H., and Willilams, K. R. (1993) *J. Mol. Biol. 232*, 89−104.
22. Qiu, H., Kaluarachchi, K., Du, Z., Hoffman, D. W., and Giedroc, D. P. (1996) *Biochemistry 35*, 4176−4186.
23. Du, Z., Giedroc, D. P., and Hoffman, D. W. (1996) *Biochemistry 35*, 4187−4198.
24. Holland, J. A., Hansen, M. R., Du, Z., and Hoffman, D. W. (1998) *RNA 4* (in press).
25. Stein, A., and Crothers, D. M. (1976) *Biochemistry 15*, 160−168.
26. Laing, L. G., Gluick, T. C., and Draper, D. E. (1994) *J. Mol. Biol. 237*, 577−587.
27. Schellman, J. A. (1975) *Biopolymers 14*, 999−1018.
28. Hill. T. L. (1957) *J. Polym. Sci. 23*, 549−562.
29. Wyman, J., and Gill, S. J. (1990) in *Binding and Linkage. Functional Chemistry of Biological Macromolecules*, University Science Books, Mill Valley, CA.
30. Turner, D. H., Sugimoto, N., and Freier, S. M. (1988) *Annu. Rev. Biophys. Biophys. Chem. 17*, 167−192.
31. Fresco, J. R., Klotz, L. C., and Richards, E. G. (1963) *Cold Spring Harbor Symp. Quant. Biol. 28*, 83−90.
32. Record, M. T., Jr., Lohman, T. M., and de Haseth, P. (1976) *J. Mol. Biol. 107*, 145−158.
33. Crothers, D. M., Cole, P. E., Hilbers, C. W., and Shulman, R. G. (1974) *J. Mol. Biol. 87*, 63−88.
34. Wyatt, J. R., Puglisi, J. D., and Tinoco, I., Jr. (1990) *J. Mol. Biol. 214*, 455−470.

BI981726Z